AFRL-ML-WP-TP-2007-530

ASYMMETRY IN PLATINUM ACETYLIDE COMPLEXES: CONFINEMENT OF THE TRIPLET EXCITON TO THE LOWEST ENERGY LIGAND (PREPRINT)

Thomas M. Cooper, Douglas M. Krein, Aaron R. Burke, Daniel G. McLean, Joy E. Rogers, and Jonathan E. Slagle

Hardened Materials Branch
Survivability and Sensor Materials Division

AUGUST 2006

Approved for public release; distribution unlimited.

See additional restrictions described on inside pages

STINFO COPY

AIR FORCE RESEARCH LABORATORY
MATERIALS AND MANUFACTURING DIRECTORATE
WRIGHT-PATTERSON AIR FORCE BASE, OH 45433-7750
AIR FORCE MATERIEL COMMAND
UNITED STATES AIR FORCE

NOTICE AND SIGNATURE PAGE

Using Government drawings, specifications, or other data included in this document for any purpose other than Government procurement does not in any way obligate the U.S. Government. The fact that the Government formulated or supplied the drawings, specifications, or other data does not license the holder or any other person or corporation; or convey any rights or permission to manufacture, use, or sell any patented invention that may relate to them.

This report was cleared for public release by the Air Force Research Laboratory Wright Site (AFRL/WS) Public Affairs Office and is available to the general public, including foreign nationals. Copies may be obtained from the Defense Technical Information Center (DTIC) (http://www.dtic.mil).

AFRL-ML-WP-TP-2007-530 HAS BEEN REVIEWED AND IS APPROVED FOR PUBLICATION IN ACCORDANCE WITH ASSIGNED DISTRIBUTION STATEMENT.

*//Signature//

THOMAS M. COOPER, Ph.D.
Agile Limiters Project
Exploratory Development
Hardened Materials Branch

//Signature//

MARK S. FORTE, Acting Chief
Hardened Materials Branch
Survivability and Sensor Materials Division

//Signature//

TIM J. SCHUMACHER, Chief
Survivability and Sensor Materials Division

This report is published in the interest of scientific and technical information exchange, and its publication does not constitute the Government's approval or disapproval of its ideas or findings.

*Disseminated copies will show "//Signature//" stamped or typed above the signature blocks.

REPORT DOCUMENTATION PAGE

Form Approved
OMB No. 0704-0188

The public reporting burden for this collection of information is estimated to average 1 hour per response, including the time for reviewing instructions, searching existing data sources, searching existing data sources, gathering and maintaining the data needed, and completing and reviewing the collection of information. Send comments regarding this burden estimate or any other aspect of this collection of information, including suggestions for reducing this burden, to Department of Defense, Washington Headquarters Services, Directorate for Information Operations and Reports (0704-0188), 1215 Jefferson Davis Highway, Suite 1204, Arlington, VA 22202-4302. Respondents should be aware that notwithstanding any other provision of law, no person shall be subject to any penalty for failing to comply with a collection of information if it does not display a currently valid OMB control number. **PLEASE DO NOT RETURN YOUR FORM TO THE ABOVE ADDRESS**.

1. REPORT DATE *(DD-MM-YY)*	2. REPORT TYPE	3. DATES COVERED *(From - To)*
August 2006	Journal Article Preprint	

4. TITLE AND SUBTITLE

ASYMMETRY IN PLATINUM ACETYLIDE COMPLEXES: CONFINEMENT OF THE TRIPLET EXCITON TO THE LOWEST ENERGY LIGAND (PREPRINT)

5a. CONTRACT NUMBER In-house

5b. GRANT NUMBER

5c. PROGRAM ELEMENT NUMBER 62102F

6. AUTHOR(S)

Thomas M. Cooper (AFRL/MLPJ)
Douglas M. Krein and Aaron R. Burke (General Dynamics Information Technology, Inc.)
Daniel G. McLean (Science Applications International Corporation)
Joy E. Rogers (UES, Inc.)
Jonathan E. Slagle (AT&T Corporation Government Solutions)

5d. PROJECT NUMBER 4348

5e. TASK NUMBER RG

5f. WORK UNIT NUMBER M08R1000

7. PERFORMING ORGANIZATION NAME(S) AND ADDRESS(ES)

Hardened Materials Branch (AFRL/MLPJ)
Survivability and Sensor Materials Division
Materials and Manufacturing Directorate
Wright-Patterson Air Force Base, OH 45433-7750
Air Force Materiel Command
United States Air Force

General Dynamics Information Technology, Inc.
5100 Springfield Pike, Suite 509
Dayton, OH 45431

Science Applications International Corp.
Dayton, OH 45433

UES, Inc.
4401 Dayton-Xenia Road
Dayton, OH 45432

AT&T Corporation Government Solutions
Dayton, OH 45324

8. PERFORMING ORGANIZATION REPORT NUMBER

AFRL-ML-WP-TP-2007-530

9. SPONSORING/MONITORING AGENCY NAME(S) AND ADDRESS(ES)

Air Force Research Laboratory
Materials and Manufacturing Directorate
Wright-Patterson Air Force Base, OH 45433-7750
Air Force Materiel Command, United States Air Force

10. SPONSORING/MONITORING AGENCY ACRONYM(S) AFRL/MLPJ

11. SPONSORING/MONITORING AGENCY REPORT NUMBER(S) AFRL-ML-WP-TP-2007-530

12. DISTRIBUTION/AVAILABILITY STATEMENT

Approved for public release; distribution unlimited.

13. SUPPLEMENTARY NOTES

Journal article submitted to J. Phys. Chem. A. The U.S. Government is joint author of this work and has the right to use, modify, reproduce, release, perform, display, or disclose the work. PAO Case Number: AFRL/WS 06-2039, 23 Aug 2006.

14. ABSTRACT

As part of an ongoing investigation of structure-optical property relationships in platinum acetylide omplexes, we synthesized the compounds *trans*-$Pt(PBU_3)_2(C{\equiv}CC_6HS)(C{\equiv}C\text{-}C_6H_4\text{-}C{\equiv}CC_6HS)$(**PE 1-2**), *trans*- $Pt(PBU_3h(C{\equiv}CC_6HS)(C{\equiv}CC_6H_4\text{-}C{\equiv}C\text{-}C_6{\sim}\text{-}C{\equiv}CC_6Hs)$(**PEl-3**) and *trans-Pt(PBU₃h(C≡C-C₆~-C≡CC₆Hs)(C≡C*$C_6H_4\text{-}C{\equiv}C\text{-}C_6H_4\text{-}C{\equiv}CC_6Hs)$(**PE2-3**)that have different ligands on either side of the central platinum and compared their spectroscopic properties to the symmetrical compounds **PEl, PE2** and PE3. We measured trends in ground state absorption, fluorescence, phosphorescence and triplet state absorption spectra. We also performed density functional theory calculations of the triplet state geometries and energies. The ground state absorption and fluorescence spectra give evidence the singlet exciton is delocalized across the central platinum atom. In contrast, the behavior of the phosphorescence spectra suggests the triplet exciton is confined to one ligand. The phosphorescence from the asymmetric complexes comes from the lowest energy, most delocalized ligand. The triplet state geometries obtained from the density functional theory calculations show distortion on the lowest energy ligand, while the other ligand has the ground state geometry. The calculated trend in the triplet state energies agrees

Continued on reverse side

15. SUBJECT TERMS Ligand, Optical Property, Phosphorescence

16. SECURITY CLASSIFICATION OF:			17. LIMITATION OF ABSTRACT:	18. NUMBER OF PAGES	19a. NAME OF RESPONSIBLE PERSON (Monitor)
a. REPORT	b. ABSTRACT	c. THIS PAGE			Thomas M. Cooper
Unclassified	Unclassified	Unclassified	SAR	52	19b. TELEPHONE NUMBER *(Include Area Code)* N/A

Standard Form 298 (Rev. 8-98)
Prescribed by ANSI Std. Z39-18

14. ABSTRACT

very well with the experimental trend. Calculations of triplet state spin density also show the triplet exciton is confined to one ligand. In the asymmetric complexes the spin density is confined to the more conjugated, lower energy ligand. The results show Kasha's rule applies to these complexes, where following excitation and intersystem crossing, the triplet exciton moves to the lowest energy ligand.

ASYMMETRY IN PLATINUM ACETYLIDE COMPLEXES: CONFINEMENT OF THE TRIPLET EXCITON TO THE LOWEST ENERGY LIGAND

ABSTRACT

As part of an ongoing investigation of structure-optical property relationships in platinum acetylide complexes, we synthesized the compounds *trans*-$Pt(PBu_3)_2(C{\equiv}CC_6H_5)(C{\equiv}C\text{-}C_6H_4\text{-}C{\equiv}CC_6H_5)$(**PE1-2**), *trans*-$Pt(PBu_3)_2(C{\equiv}CC_6H_5)(C{\equiv}C\text{-}C_6H_4\text{-}C{\equiv}C\text{-}C_6H_4\text{-}C{\equiv}CC_6H_5)$(**PE1-3**) and *trans*-$Pt(PBu_3)_2(C{\equiv}C\text{-}C_6H_4\text{-}C{\equiv}CC_6H_5)(C{\equiv}C\text{-}C_6H_4\text{-}C{\equiv}C\text{-}C_6H_4\text{-}C{\equiv}CC_6H_5)$(**PE2-3**) that have different ligands on either side of the central platinum and compared their spectroscopic properties to the symmetrical compounds **PE1**, **PE2** and **PE3**. We measured trends in ground state absorption, fluorescence, phosphorescence and triplet state absorption spectra. We also performed density functional theory calculations of the triplet state geometries and energies. The ground state absorption and fluorescence spectra give evidence the singlet exciton is delocalized across the central platinum atom. In contrast, the behavior of the phosphorescence spectra suggests the triplet exciton is confined to one ligand. The phosphorescence from the asymmetric complexes comes from the lowest energy, most delocalized ligand. The triplet state geometries obtained from the density functional theory calculations show distortion on the lowest energy ligand, while the other ligand has the ground state geometry. The calculated trend in the triplet state energies agrees very well with the experimental trend. Calculations of triplet state spin density also show the triplet exciton is confined to one ligand. In the asymmetric complexes the spin density is confined to the more conjugated, lower energy ligand. The results show Kasha's rule applies to these complexes, where following excitation and intersystem crossing, the triplet exciton moves to the lowest energy ligand.

INTRODUCTION

There has been considerable interest in the synthesis, spectroscopy, nonlinear optics and structure-property relationships of platinum acetylides.[1-7] They are exceptional systems for investigating triplet state phenomena like ground state absorption to the triplet state, intersystem crossing, the triplet state absorption spectrum and phosphorescence.[8] In our laboratory, we have been investigating the relation between chemical structure and spectroscopic properties in platinum acetylide complexes.[1,9,10] We recently published a detailed investigation of the photophysical properties of a series of butadiynes having the formula H-(C_6H_4-C≡C)$_n$-(C≡C-C_6H_4)$_n$-H, n = 1-3 and ligands H-(C_6H_4-C≡C)$_n$-H, n = 1-3 and compared these to previous work done on a complimentary series of platinum-containing complexes having the formula *trans*-Pt((P(C_4H_9)$_3$)$_2$((C≡C-C_6H_4)$_n$-H)$_2$, n = 1-3.[1,11] More recently, we synthesized a series of half-platinum acetylide complexes having the formula *trans*-Pt(II)(PBu_3)$_2$((C≡CC_6H_4)$_n$-H)Cl, where n = 1-3.[12] In all these articles, analysis of the dependence of singlet and triplet state energies on chromophore length gives evidence that the singlet exciton is delocalized through the central platinum, while the triplet exciton is confined to one ligand.

Time-resolved infrared spectra of the triplet state *trans*-Pt(PBu_3)$_2$((C≡C-C_6H_4-C≡CC_6H_5)$_2$[13] give evidence the triplet state geometry has cumulenic and quinone character. A related time-resolved infrared spectroscopy and theoretical study of *trans*-Pt(PBu_3)$_2$(C≡CC_6H_5)$_2$ gives evidence the triplet exciton is confined to one ligand.[6] A theoretical study of the same compound also suggests the triplet state is confined to one ligand.[14] A suggested intersystem crossing mechanism in platinum acetylides involves an

initial delocalized singlet state exciton converting to a triplet exciton confined to one ligand.

In this paper we describe the synthesis and characterization of three platinum acetylides *trans*-$Pt(PBu_3)_2(C{\equiv}CC_6H_5)(C{\equiv}C\text{-}C_6H_4\text{-}C{\equiv}CC_6H_5)$(**PE1-2**), *trans*-$Pt(PBu_3)_2(C{\equiv}CC_6H_5)(C{\equiv}C\text{-}C_6H_4\text{-}C{\equiv}C\text{-}C_6H_4\text{-}C{\equiv}CC_6H_5)$(**PE1-3**) and *trans*-$Pt(PBu_3)_2(C{\equiv}C\text{-}C_6H_4\text{-}C{\equiv}CC_6H_5)(C{\equiv}C\text{-}C_6H_4\text{-}C{\equiv}C\text{-}C_6H_4\text{-}C{\equiv}CC_6H_5)$(**PE2-3**) that have different ligands on either side of the central platinum. These compounds have C_s symmetry and we compare their spectroscopic properties to the C_{2h} symmetry compounds **PE1**, **PE2** and **PE3**. The nomenclature is described in Figure 1. With the lower symmetry we can distinguish between two possible intersystem crossing mechanisms where the triplet exciton goes to either ligand or preferentially goes to one ligand. We found the singlet exciton to be delocalized throughout the molecule, while the triplet exciton to be confined to the lowest energy ligand. We also did density functional theory(DFT) calculations on the ground and lowest triplet state of **PE1**, **PE2**, **PE3**, **PE1-2**, **PE1-3** and **PE2-3**. The experimental trends were reproduced very well by the DFT calculations.

GENERAL SYNTHESIS METHODS

All reactions were carried out using dry, distilled solvents and under dry, high purity nitrogen. All reagents were purchased from Aldrich Chemical Company and used without further purification. Reverse phase column refers to Alltech Extract-Clean C18. The ligands **PE2-H** and **PE3-H** and compounds $Pt(C{\equiv}C\text{-}C_6H_5)Cl(PBu_3)_2$ (**half-PE1**), $Pt(C{\equiv}C\text{-}C_6H_4\text{-}C{\equiv}C\text{-}C_6H_5)Cl(PBu_3)_2$ (**half-PE2**), $Pt(C{\equiv}CC_6H_4C{\equiv}CC_6H_5)_2(PBu_3)_2$ (**PE2**)

and $Pt(C{\equiv}CC_6H_4C{\equiv}CC_6H_4C{\equiv}CC_6H_5)_2(PBu_3)_2$ (**PE3**) were synthesized as described previously.[1,12]

SYNTHESIS

$Pt(C{\equiv}CC_6H_5)(C{\equiv}CC_6H_4C{\equiv}CC_6H_5)(PBu_3)_2$ (**PE1-2**) In a 100 ml three-neck round-bottom flask 480 mg(0.6535 mmol) of **half-PE1** was dissolved in 35 ml of diethyl amine, followed by addition of 12.5 mg of CuI and 133 mg (0.6535 mmol) of **PE2-H.** The solution was heated to reflux and stirred overnight. The solvent was removed on a rotovap and the remaining solid was then dissolved in DCM and adsorbed to a small amount of silica gel. This was layered over a 4 inch column of silica gel and eluted with first hexane and then a then varying percentages of a hexane/DCM mixture. Approximately 200 mg of the light yellow solid product was isolated. MA: found C, 64.18; H, 7.36%. $C_{48}H_{68}P_2Pt$ requires C, 63.91; H, 7.60%; MW =901; IR: (KBr, thin film) 2,099 cm^{-1} ν(Pt-C≡C), ^1H NMR ($CDCl_3$): δ 0.96 (m, 18H, CH_3), 1.47 (m, 12H, CH_2), 1.60 (m, 12H, CH_2), 2.17 (m, 12H, CH_2), 7.25 – 7.40 (m, 14H, ArH) ppm. ^{13}C NMR ($CDCl_3$): δ 14.09 (s, CH_3), 23.96 (t, *J*(CP) = 17 Hz, CH_2), 24.19 (t, *J*(CP) = 7 Hz, CH_2), 24.68 (t,, J(CP)=7 Hz, CH_2), 26.64, (s, CH3), 108.0(t, J(CP) = 14 Hz, Pt-C≡C), 112.4(t, J(CP) = 14 Hz.Pt-C≡C), 90.0(s, C≡C), 90.4(s, C≡C), 109.3(s, C≡C), 109.4(s, C≡C), 119.4, 123.9, 125.1, 128.1, 128.3, 128.6, 129.3, 129.5, 130.9, 131.0, 131.5, 131.7 (Ar) ppm; ^{31}P NMR ($CDCl_3$): δ (s and d centered at δ4.25, *J*(PPt) = 2351 Hz, PBu_3) ppm. EIMS: (m/z) 901.

$Pt(C{\equiv}CC_6H_5)(C{\equiv}CC_6H_4C{\equiv}CC_6H_4C{\equiv}CC_6H_5)(PBu_3)_2$ (**PE1-3**) In a 100 ml three-neck round-bottom flask 418 mg (0.5721 mmol) of **half-PE1** was dissolved in 40 ml of diethyl

amine, followed by addition of 12.5 mg of CuI and 173 mg (0.5721 mmol) of **PE3-H**. The solution was heated to reflux and stirred overnight. The solvent was removed on a rotovap and the remaining solid was then dissolved in DCM and adsorbed to a small amount of silica gel. This was layered over a 4 inch column of silica gel and eluted with first hexane and then a then varying percentages of a hexane/DCM mixture. Two fractions of the hexane/DCM eluents showed a mixture of product and **PE1** by NMR. These mixtures were combined and put through a one inch reverse phase column using acetonitrile then DCM as eluents. Approximately 130 mg of a waxy light yellow solid was isolated in an acetonitrile/DCM fraction. MA: found C, 67.68; H, 6.90%. $C_{56}H_{72}P_2Pt$ requires C, 67.11; H, 7.24%; MW =1001; IR: (KBr, thin film) 2096 cm^{-1} ν(Pt-C≡C), ^1H NMR ($CDCl_3$): δ 0.99 (m, 18H, CH_3), 1.49 (m, 12H, CH_2), 1.66 (m, 12H, CH_2), 2.19 (m, 12H, CH_2), 7.29 – 7.55 (m, 18H, ArH) ppm. ^{13}C NMR ($CDCl_3$): δ 14.15 (s, CH_3), 24.19 (t, *J*(CP) = 17 Hz, CH_2), 24.64 (t, *J*(CP) = 7 Hz, CH_2), 24.82 (s, CH_2), 26.66, (s, CH3), 107.96(t, J(CP) = 14 Hz, Pt-CC), 112.89(t, J(CP) = 14 Hz, Pt-C≡C), 89.5(s, C≡C), 89.9(s, C≡C), 91.5(s, C≡C), 92.4(s, C≡C), 109.4(s, C≡C), 109.5(s, C≡C), 119.2, 123.1, 123.4, 123.7, 125.2, 128.2, 128.7(br), 129.3, 129.7, 131.1(br), 131.6, 131.7, 131.8, 131.9 (Ar) ppm.; ^{31}P NMR ($CDCl_3$): δ (s and d centered at δ4.26, *J*(PPt) = 2351 Hz, PBu_3) ppm. EIMS: (m/z) 1001.

$Pt(C{\equiv}CC_6H_4C{\equiv}CC_6H_5)(C{\equiv}CC_6H_4C{\equiv}CC_6H_4C{\equiv}CC_6H_5)(PBu_3)_2$ (**PE2-3**) In a 100 ml three-neck round-bottom flask 546 mgs (0.653 mmol) of **half-PE2** was dissolved in 50 ml of diethyl amine, followed by addition of 12.5 mg of CuI and 157.5 mgs (0.521 mmoles) of **PE3-H** and the mixture stirred for four days at room temperature. The solvent was

removed on a Rotovap and the remaining solid was then dissolved in DCM and occluded to a small amount of silica gel. This was layered over a 4 inch column of silica gel and eluted with first hexane and then a then varying percentages of a hexane/DCM mixture. The fraction eluted with a hexane/25%DCM mixture contained the product with a small amount of **half-PE2**. This fraction was put through a one inch reverse phase using methanol and varying MeOH/DCM mixtures as the eluent. Approximately 280 mgs of a waxy light yellow solid was isolated from the MeOH/25%DCM fraction. MA: found C, 69.71; H, 6.69%. $C_{64}H_{76}P_2Pt$ requires C, 69.73; H, 6.95%; MW =1101; IR: (KBr, thin film) 2095 cm^{-1} ν(Pt-C≡C), ^1H NMR ($CDCl_3$): δ 0.97 (m, 18H, CH_3), 1.49 (m, 12H, CH_2), 1.66 (m, 12H, CH_2), 2.19 (m, 12H, CH_2), 7.26 – 7.60 (m, 22H, ArH), ^{13}C NMR ($CDCl_3$): δ 14.10(s, CH3), 24.47(t, J(CP) = 17 Hz, CH2), 24.69(t, J(CP) = 17 Hz, CH2), 26.65(s, CH3) ppm, 111.9(t, J(CP = 14 Hz, Pt-C≡C), 112.5(t, J(CP) = 14 Hz, Pt-C≡C), 109.7(s, br, C≡C), 89.5(s, C≡C), 89.9(s, C≡C), 90.1(s, C≡C), 90.3(s, C≡C), 91.4(s, C≡C), 92.3(s, C≡C), 119.2, 119.5, 123.1, 123.4, 123.7, 123.8, 128.3, 128.6, 128.79br), 129.4, 129.6, 131.0(br), 131.50, 131.54, 131.65, 131.74, 131.8, 131.9 (Ar) ppm ^{31}P NMR ($CDCl_3$): δ (s and d centered at δ4.34, J(PPt) = 2351 Hz, PBu_3) ppm. EIMS: (m/z) 1101.

COMPUTATIONAL METHODS

Calculations were done using Gaussian 03W, version 6.1.[15] The presence of the heavy platinum center required a basis set that includes relativistic effects through an effective core potential. We used density functional theory(DFT) with the B3LYP functional and the relativistic LANL2DZ basis set.[16,17] To save computer time, the phosphine portion of the molecule was converted from tributyl phosphine to trimethyl phosphine. We performed geometry optimizations for the ground and T_1 states. For the

ground state, energy minimizations were performed with the symmetrical complexes **PEn** having the ligand plane perpendicular to the P-Pt-P axis, constraining the symmetry to C_{2h} and the asymmetric complexes **PEa-b** to C_s. We used DFT to calculate the T_1 state geometry of the triplet state. DFT is known as a ground state theory only rigorously valid for the ground state of a given symmetry (including spin symmetry).[18] In this instance the T_1 state is the "ground state". Our starting geometry for these minimizations was that previously found for **PE1**,[14] where the ligand plane was parallel to the P-Pt-P axis and the symmetry allowed to be C_1. We used the ΔSCF method to estimate E_T as given by the expression

E_T = E(Triplet state relaxed geometry) – E(Ground state relaxed geometry).

The singlet excited states were investigated by density functional response theory(TDDFT), where the 6 lowest singlet roots were obtained.

GENERAL SPECTROSCOPY TECHNIQUES

All absorption and fluorescence spectra were obtained in benzene solutions. Ground state UV/Vis absorption spectra were measured on a temperature-controlled Cary 500 spectrophotometer. Emission spectra at 5 nm slit width were measured using a Perkin-Elmer model LS 50B fluorometer. Low-temperature phosphorescence was done in methyltetrahydrofuran as a frozen glass at 77 K and exciting at 350 nm. Nanosecond transient absorption measurements were carried out using the third and fourth harmonics (355 nm and 266 nm) of a Q-switched Nd:YAG laser (Quantel Brilliant, pulse width ca. 5 ns). All samples were deoxygenated with three freeze-pump-thaw cycles. Pulse fluences of up to 8 mJ cm^{-2} are typically used at the excitation wavelength. Ground state absorption spectra were obtained before and after the flash photolysis experiment. Most

samples showed less than 10% degradation. If necessary, spectra were collected from photosensitive samples by collecting the spectrum in a 100 nm increment and then putting a fresh sample into the instrument. A detailed description of the laser flash photolysis apparatus has been published.[1]

RESULTS

Table 1 lists selected ^{13}C NMR data for the mixed compounds. The table lists the chemical shift for the Pt-C carbon. Also included are corresponding chemical shifts for the **PEn** complexes that have been previously published.[19] The magnitude of the shifts were similar to those seen in the symmetric complexes. For example, δ(**PE1-2**, ligand 1) ~ δ(**PE1**), and δ(**PE1-2**, ligand 2) ~ δ(**PE2**). The chemical shifts for the asymmetric complexes split into two values. For a complex **PEab**, the interaction between ligands **a** and **b** is determined by calculating the difference

$$\Delta_{ab} = \delta_a - \delta_{aa}$$

and

$$\Delta_{ba} = \delta_b - \delta_{bb},$$

where δ_a is the chemical shift of the Pt-C carbon of ligand **a** of the complex and δ_{aa} is the corresponding chemical shift for the complex **PEa**. Δ_{ab} is the influence of ligand **b** on ligand **a**. Similarly, the value Δ_{ba} is calculated from values for ligand **b** of the complex and the complex **PEb**. For a complex **PEa-b**, the interaction effect caused a small upfield shift in the left ligand **a** and a corresponding small downfield shift in the right ligand **b**. The magnitude of Δ behaves as **PE1-3** ~ **PE1-2** > **PE2-3**. The dipole moment calculated by DFT follows a similar ordering: μ(**PE1-3**) > μ(**PE1-2**) > μ(**PE2-3**).

In Figure 2, the absorption spectrum of **PE1-2** has an absorption maximum of 349 nm, while that for **PE1-3** red-shifts to 357 nm. The band shape and absorption maximum of **PE2-3** are identical to those of **PE1-3**, although its spectrum has an increased extinction coefficient, as given in Table 2. All three absorption spectra have at least two closely-spaced bands near the absorption maximum. A Gaussian fit of the spectra shows the spacing between the two bands is ~0.2 eV. The oscillator strengths increase according to the order f(**PE1-2**) < f(**PE1-3**) < f(**PE2-3**). The behavior of the fluorescence spectra mirrors that of the absorption spectra, with **PE1-2** blue shifting from **PE1-3** and **PE2-3**, both of which have similar emission spectra. Unlike the absorption spectra, each of the emission spectra have only one band and do not show distinct vibronic structure.

The triplet state absorption spectra(Figure 3) are similar to ground state absorption and emission spectra. **PE1-2**'s spectrum is blue-shifted from **PE1-3** and **PE2-3**, which are nearly identical. All three spectra have a major band: 590 nm for **PE1-2** and 650 nm for **PE1-3** and **PE2-3** as well as a minor band: ~485 nm for **PE1-2** and 525 nm for **PE1-3** and **PE2-3**. The bleaching region shows **PE1-2** bleaching at ~350 nm, while **PE1-3** and **PE2-3** bleach at ~370 nm. The average energy difference between the two bands is ~0.4 eV.

We collected phosphorescence spectra of **PE1-2**, **PE1-3** and **PE2-3** and compared these spectra to phosphorescence from **PE2** and **PE3**(Figure 4). We find that the phosphorescence spectrum of **PE1-2** to be identical to that of **PE2**, and the spectrum of **PE1-3** and **PE2-3** to be identical to that of **PE3**. In the **PE2-3** emission spectrum, we also observe a weak emission attributable to the 0-0 emission band from the **PE2** ligand. Table 2 summarizes data obtained from ground state absorption and emission spectra.

Table 3 lists all the state energies plus previously published state energy data for **PE1**, **PE2** and **PE3** [1,11]. The trend in state energies for E_S is: **PE1** > **PE1-2** > **PE2** > **PE1-3** ~ **PE2-3** ~ **PE3**. The trend for the E_T state energy is: **PE1** > **PE1-2** = **PE2** > **PE1-3** = **PE2-3** = **PE3**. With the exception of **PE1**, all ΔE_{ST} values are around 1 eV. The E_{TT} values follow the trend **PE1-2** ~ **PE2** > **PE1-3** ~ **PE2-3** ~ **PE3**.

Table 4 lists results of various calculations. Listed is the ground state energy after geometry optimization and the corresponding energy of the triplet-state-optimized geometry. As a test of our method, we did similar ΔSCF calculations for the monosubstituted **half-PEn** chromophores and compared them to experimental E_T values.[12] For the **half-PEn** compounds, we found the calculated(experimental) E_T values to be **half-PE1**: 2.88(2.92); **half-PE2**: 2.32(2.39); **half-PE3**: 2.17(2.28). By calculating the difference between the two energies, we determine the E_T trend to be **half-PE1** ~ **PE1** > **half-PE2** = **PE2** = **PE1-2** > **half-PE3** = **PE1-3** = **PE2-3** = **PE3**. The calculated triplet state dipole moments follow the trend **PE1** < **PE2** < **PE1-2** < **PE3** < **PE2-3** < **PE1-3**. E_S is estimated from the lowest-lying allowed transition having oscillator strength greater than 0.1. The supplementary material lists all the electronic states obtained from the TDDFT calculation. The next most intense state is about 0.3-0.4 eV higher in energy with 70-80% lower oscillator strength. The E_S values follow the trend **PE1** > **PE1-2** > **PE2** >**PE1-3** ~ **PE2-3** ~ **PE3**. The oscillator strengths order according to **PE1** < **PE1-2** < **PE1-3** < **PE2-3** < **PE2** < **PE3**. Examination of the CI coefficients show the largest configuration of this state is a HOMO → LUMO transition.

Figure 5 shows a plot of the calculated *vs.* measured E_S and E_T values. A plot of E_T(experimental) *vs.* E_T(calculated) have an excellent linear correlation. The linear fit gives the expression(in eV),

$$E_T(expt)(eV) = 0.4758 + 0.8228\ E_T(calc),\ r = 1.$$

A similar plot for E_S gives the expression

$$E_S(expt)(eV) = 2.3014 + 0.3048\ E_S(calc),\ r = 0.9649.$$

Although there is a lower correlation, the calculated E_S predicts the correct ordering of state energies with chromophore size.

Figure 6 shows images of the HOMO and LUMO for the chromophores. Neglecting the phosphines, **PE1**, **PE2** and **PE3** have D_{2h} symmetry. The HOMO consists of p orbitals on each of the phenyl acetylene units and a d orbital on the platinum and had b_{2g} symmetry. The nodes cut through the bonds. Each phenyl acetylene unit has two nodes, one through the phenyl group and one through the phenyl acetylene carbon-carbon bond. There is another node between the platinum-carbon bond and a node between the lobes of the d orbital on the platinum atom. The LUMO consists of p orbitals on the phenyl acetylene units and an empty d orbital on the platinum and has b_{3u} symmetry. The nodes cut through the bonds. Each phenyl acetylene unit has three nodes, two in the phenyl group and one bisecting the acetylene group. There is another node bisecting the Pt-C bond and the Pt d orbital. An allowed HOMO $\rightarrow$ LUMO transition is the z-polarized B_{1u} state and is assigned as an ^1L_a state.[20-22] In **PE1**, there are 7 nodes in the HOMO, and 6 in the LUMO, showing the allowed optical transition followa the $\Delta q = \pm 1$ selection rule, as well as the g $\rightarrow$ u rule. The same analysis holds true for **PE2** and **PE3**.

Neglecting the phosphines in **PE1-2**, **PE1-3** and **PE2-3**, the chromophores have C_{2v} symmetry. Both B_{2g} and B_{3u} representations in D_{2h} transform as B_1 in C_{2v}. Similarly, both A_g and B_{1u} representations in D_{2h} transforms as A_1 in C_{2v}. Like the **PEn** complexes, the HOMO consists of p orbitals on the phenyl acetylene groups and a d orbital on the platinum and had b_1 symmetry. By looking at the "inversion" symmetry through the platinum atom, the p orbitals of corresponding atoms on opposite sides of the ligand have the same sign, giving them "g" symmetry. In **PE1-3** and **PE2-3** there is less electron density on the outer phenyl of the **PE3** ligand. The phenyl acetylene node pattern is the same as seen in the **PEn** complexes. The LUMO consists of p orbitals on the phenyl acetylene units and smaller contribution from the d orbital on the platinum atom and has b_1 symmetry. The "inversion" symmetry through the platinum atom shows the p orbitals of corresponding atoms on opposite sides of the ligand have opposite signs, giving them "u" symmetry. Since the d orbital has "g" symmetry, there is bonding between the platinum d orbital and one of the acetylene p orbitals. As in **PEn**, each phenyl acetylene unit has three nodes. An allowed HOMO → LUMO transition is a z-polarized A_1 state. In **PE1-2** the HOMO has 10 nodes, and the LUMO has 11 nodes, showing a $\Delta q = \pm 1$ selection rule. Analysis of the p orbital signs shows "g" → "u" character in the HOMO → LUMO transition. Similar analyses hold true in **PE1-3** and **PE2-3**.

Table 5 summarizes ground and triplet state geometry data. The table shows ground and triplet state bond lengths for the right ligand. For a given number of phenylacetylene units in a ligand, the ground and triplet state geometries in both the left and right ligands are the same. The average ground state acetylene bond length, 1.23 Å, is

close to the standard bond length of 1.20 Å. The bonds R_3, R_7, R_9, R_{13} and R_{15} have an average length of 1.43 Å, making them intermediate between a single bond(1.54 Å) and a double bond(1.36 Å). The average bond length in the phenyl rings is 1.41 Å , close to the standard length for a benzene carbon-carbon bond(1.39 Å). In the geometry optimizations, the **PE** ligand is constrained to be planar. A published X-ray structure of **PE2** gives R_2 = 1.214Å and R_8 = 1.199Å[4] *vs.* our calculated values of 1.243 Å and 1.229 Å. Our calculated bond lengths are 0.03 Å larger than the experimental values, but there is good agreement for the difference between R_2 and R_8, 0.015 Å. In the triplet state, the acetylene bond lengths increase, while the adjoining carbon-carbon bonds decrease in length, giving the linkage more allenic character. There are also decreases in the 2'-3' bond lengths, while the 1'-2' and 3'-4' lengths increase. The net result of these changes give the ligand more quinone character. The largest RMS bond length changes occur in **PE1**, with smaller changes in larger ligands. To estimate ligand flexibility, we calculate the barrier to rotation about the phenyl acetylene linkage in the **PE2-H** ligand to be 1.6 kcal/mole. The rotation barrier of the **PE2-H** ligand in the triplet state is estimated to be 9.4 kcal/mole.

Figure 7 shows plots of the spin density of the triplet state. The chromophores are divided into the individual phenyl acetylene units of either the left or right ligand, and the central platinum/phosphine units. With the exception of **PE1**, having a spin density of 0.20, there is no significant spin density on the platinum/phosphine unit. For all the compounds, the left ligand has virtually no spin density. Instead, most of the spin density is confined to the right ligand. In the asymmetric complexes, the triplet exciton is confined to the larger, lower energy ligand. The magnitude of the spin density is only a

function of the right ligand size. The spin densities are identical in **PE1-2** and **PE2**. The spin densities of the right ligands of **PE1-3**, **PE2-3** and **PE3** are also identical. As the length of the right ligand increases from one to three phenyl acetylene units, the spin density of the phenyl acetylene nearest the platinum atom decreases from 1.70 to 0.25. The spin density of the second phenyl acetylene unit increases from 0.59 to 0.95. The spin density on the third phenyl acetylene unit is 0.73. The average spin density per functional group follows the trend Pt/phosphine, 0.086; ethynyl, 0.694 and phenyl, 1.22. As a comparison, a geometry optimization for the T_1 state of the butadiyne **PE1-BD**(C_6H_5-C≡C-C≡C-C_6H_5) shows the spin densities are symmetrically placed throughout the molecule, with the acetylenic carbons having a spin density of 1.064 and the phenyl groups having a spin density of 0.936.

DISCUSSION

An issue that has been investigated by our group as well as other groups is the relation between molecular structure and the delocalization of the singlet and triplet excitons. A theoretical and experimental investigation of the polymer poly($Pt(PBu_3)_2(C{\equiv}CC_6H_4)$) finds the triplet exciton T_1 is localized on a single phenylene ring while the S_1 and T_n excitons are delocalized over several monomer units.[23] The spectra of a series of oligomers having the formula $C_6H_5(C{\equiv}C\text{-}Pt(PBu_3)_2\text{-}C{\equiv}CC_6H_4)_n\text{-}H$, n=1-5, 7 shows similar trends.[2] The ground state absorption and fluorescence spectra show systematic red shifts as the oligomer length increases. In contrast, the phosphorescence spectra show only small red shifts with increasing oligomer length. The results support the idea that the triplet state is more localized than the singlet state. An

investigation of the photophysics and photochemistry of platinum acetylide stilbenes gives evidence that triplet state resides on one ligand.[24]

Our group has done several previous studies on the relationship between platinum acetylide length and singlet state energy, including *trans*-Pt(II)$(PBu_3)_2((C{\equiv}CC_6H_4)_n$-$H)_2$, where n = 1-3,[1] their analogous butadiynes H-$(C_6H_4$-$C{\equiv}C)_n$-$(C{\equiv}C$-$C_6H_4)_n$-H, n = 1-3, [11] the monosubstituted complexes Pt(II)$(PBu_3)_2((C{\equiv}CC_6H_4)_n$-H)Cl, where n = 1-3[12] and sydnone-containing complexes.[19] In all these studies the singlet state energy E_S decreases as the molecular length increases. Our TDDFT calculations also show the calculated E_S values correlate well with the experimental values. There does appear to be a limit to the conjugation length, as the state energies of **PE1-3**, **PE2-3** and **PE3** are about the same, a trend also seen in the TDDFT calculations. The large measured oscillator strengths of the low-lying transitions suggest there are multiple electronic states in the absorption spectrum. Our calculations show a weaker transition 0.3-0.4 eV higher in energy than the intense low-lying state, giving evidence for higher states in the ground state spectrum. The lowest energy allowed transition to the singlet state has HOMO → LUMO character. The HOMO is delocalized throughout the chromophore, with contribution from phenyl acetylene p orbitals and a d orbital on the platinum, while the LUMO has mixed MLCT and ligand-ligand charge transfer character. Both the HOMO and the LUMO are delocalized throughout the chromophore.

In contrast, the behavior of the triplet state energy E_T shows the triplet exciton is confined to one ligand. This has been shown in the monosubstituted complexes, where the triplet state energy E_T of Pt(II)$(PBu_3)_2((C{\equiv}CC_6H_4)_n$-H)Cl is the same as the corresponding symmetric complexes.[12] In the present work, we have shown that the

phosphorescence of mixed complexes **PEa-b** is identical to that of the symmetric complexes **PEb**, where b is the more conjugated ligand. Our DFT calculations show a strong correlation between calculated and experimental E_T, supporting this observation. The triplet state geometry and spin density results both show the triplet state is confined to one ligand and to the more conjugated ligand in the **PEa-b** complexes. The calculations show the confinement of the spin to one ligand results in a significant triplet state dipole moment resulting from the charge transfer character of the triplet exciton.

To gain more insight into the electronic states of these chromophores, we ran TDDFT calculations. In all these chromophores the lowest excited singlet state has significant HOMO → LUMO character. The only exception is **PE1**, which also has HOMO -1 → LUMO+1 character. As has been shown in previous experimental and theoretical studies, the HOMO consists of π orbitals residing on the phenyl acetylene units and 5d orbitals on the platinum. The LUMO consists of π* orbitals on the ligands with the central d orbital empty. Notably, in the asymmetric **PEa-b** chromophores, the optical transitions have charge transfer character. In **PE1-2**, the HOMO is delocalized over the entire molecule. The ^{13}C NMR data and DFT calculations give evidence of a ground state dipole moment, where the interaction effect on the chemical shift is largest in the most asymmetric **PE1-3**, but smallest in **PE2-3**. The dipole moment trend shows the larger difference between the ligands in **PEa-b** complexes, the larger the dipole moment. In the LUMO, the ligand **1** has less electron density and more of the excitation is confined to ligand **2**. Similar behavior is seen in **PE1-3** and **PE2-3**. The HOMO is delocalized across the platinum atom, while the LUMO consists of the larger ligand. From these results we conclude the main optical transition in **PEa-b** is MLCT with

ligand-to-ligand charge transfer character. In the literature, the asymmetrical complexes $Pt(C{\equiv}CC_6H_4OCH_3)(C{\equiv}CC_6H_4NO_2)(PBu_3)_2$ and $(Pt(C{\equiv}CC_6H_4N(CH_3)_2)(C{\equiv}CC_6H_4NO_2)(PBu_3)_2$ have been shown to have dipole moments of 5D.[25]

We find the average singlet-triplet splitting to be 1.0 eV in our compounds. This value contrasts to a ΔE_{ST} of 0.7 eV in polymeric platinum acetylide complexes.[3] The energy is proportional to the overlap integral between the singlet and triplet excitons. Because the singlet state exciton is more confined in our chromophores than in the polymeric systems, it results in a larger energy gap.

We found DFT to be a successful method to calculate E_T. This is an application of the ΔSCF method, where density functional techniques are used to investigate the lowest lying state of a given spin.[18] This result supports previous theoretical work, [26], where DFT was successfully used to calculate E_T. In agreement with that work, our calculated E_T values were within 0.1 eV of the experimental values. Our calculations of E_T of the **half-PEn** compounds also agree within 0.1 eV of experiment, providing further support for this method to describe the triplet state. Out triplet state geometry calculations build upon previous investigations of **PE1**.[14] They show the triplet state of **PE1** to have significant geometry distortion from the ground state. The distortion occurs on one ligand. We also find the triplet state symmetry to be lower than the ground state, with the spin density confined to one of the ligands. In the **PEa-b** compounds, the spin density is confined to the largest ligand. Combined with the experimental phosphorescence spectra, the current results show that in **PEn** compounds, the triplet state is confined to one ligand. In **PEa-b** compounds, the triplet state is confined to the largest ligand. The potential energy barrier calculations we performed on **PE2-H** give

evidence the ligand portion of the triplet state is planar. A recently synthesized **PE1-hexabenzocoronene** shows a phosphorescence band at 578 nm from the hexabenzocoronene ligand and no emission from the **PE1** ligand.[27] Similar evidence of confinement of the triplet exciton to the core of a series of branched platinum acetylide complexes rather than the outer **PE1**-like ligands has been described.[28] All these results derive from Kasha's rule, where emission occurs from the lowest energy electronically excited state of the molecule. This behavior is observed in **PE1-2** and **PE1-3**, where the energy of ligand **1** is considerably higher than the other ligand. However, in **PE2-3**, we observe a small emission from ligand **2** ligand. The energy difference between the 0-0 bands of the two ligands(0.12 eV) is small enough that during intersystem crossing, some of the excitation goes to ligand **2**.

In contrast to the behavior of the phosphorescence spectra, the $T_1 \rightarrow T_n$ transition red-shifts with increasing chromophore size.[1,11] A comparison of the $T_1 \rightarrow T_n$ transition energy of the **PEn** chromophores vs. the monosubstituted **half-PEn** chromophores give evidence this is an LMCT transition delocalized across the platinum center.[12] In the current work, the $T_1 \rightarrow T_n$ transition shows increased conjugation when comparing **PE1-2** and **PE1-3**, but the T_n state conjugation length of **PE2-3** is the same as that of **PE1-3**.

The expression for the intersystem crossing rate constant can be used to analyze the factors underlying the conversion from the singlet to triplet state.[29,30]

$$k_{isc} = k_{\max} \frac{\langle S_1 | H_e | T_1 \rangle^2}{\Delta E^2} \frac{\langle S_1 | H_{so} | T_1 \rangle^2}{\Delta E^2} \langle \chi_{S_1} | \chi_{T_1} \rangle^2$$

This equation describes the interactions between S_1 and T_1 contributing to the rate of intersystem crossing. The first term describes electronic interactions. The second term describes spin-orbit coupling and the third term describes Franck-Condon factors.

Our experiments involve excitation of these chromophores initially in the ground state and observing the steady state and time-resolved behavior of the triplet state. We have previously shown the singlet state lifetime of these compounds is less than 30 ps and the intersystem crossing quantum yield is nearly unity.[1] Our calculations give good information about the S_0 state, the Franck-Condon S_1 state, and the T_1 state. We currently have no information about the S_1 and T_1 potential energy surfaces and the dynamics underlying the intersystem crossing process. The transitions are most probable at geometries where the energy difference between the surfaces is small, and there is a strong electronic and vibrational interaction between the S_1 and T_1 states. These critical geometries may correspond to an avoided crossing minimum or a conical intersection between the S_1 and T_1 surfaces where a nonadiabatic transition will occur.[30-34] Theoretical calculation of excited state dynamics in phenylacetylene[35] and diphenylacetylene [36, 37] suggest the formation of stilbene-like biradicaloid S_1 state prior to the nonadiabatic jump to the T_1 state. This type of mechanism may occur in platinum acetylide complexes, where the initial D_{2h} symmetry Franck-Condon S_1 state relaxes to a biradicaloid state with the angle C(phenyl) – C≡C approaches 120 deg, followed by conversion to the triplet state. A time-resolved infrared spectroscopy study of **PE1** shows a splitting of the Pt-C≡C stretch vibration into two peaks, suggesting the intersystem crossing mechanism includes symmetry breaking from the S_1 state D_{2h} to T_1 state C_{2v}.[6] The authors of this paper propose the intersystem crossing process occurs by coupling of S_1 state B_{3u} symmetry PtC≡C antisymmetric stretch vibration to two uncoupled A_1 modes in the T_1 state. One of these bands is a new band at 1740 cm^{-1} and another band at a slightly higher frequency from the ground state PtC≡C stretch band. Similarly, in **PE2**,

upon formation of the triplet state, a new band appears at 1820 cm^{-1} and evidence for a similar higher frequency PtC≡C stretch band.[13] This lower frequency band has been assigned as a cumulated C=C=C stretch band. Both of these studies suggest significant structure changes in the triplet state occurs in the ethynyl groups leading to conversion from aromatic ethynyl linkages C(aromatic)-C≡C-C(aromatic) to allenic linkages(C(phenyl)=C=C=C(phenyl)). The bond length data given in Table 5 support this. The bonds undergoing greater than RMS length change between the ground and triplet state in the right ligand are R_2 to R_4 in **PE1**, R_3 to R_7 in **PE1-2** and **PE2** and R_6,R_7, R_9 and R_{10} in **PE1-3**, **PE2-3** and **PE3**. All of these geometry changes involve the bonds joining the phenyl groups. There are smaller distortions with the phenyl groups involving conversion from aromatic to quinone character.

The electronic structures of the S_1 and T_1 states are very different. For all these chromophores, the significant low-lying electronic transition has HOMO → LUMO character. The HOMO is delocalized throughout the chromophore. In **PE1**, **PE2** and **PE3**, the LUMO is also delocalized throughout the chromophore. The triplet state is confined to one ligand in all these chromophores. The intersystem crossing process involves movement of the excited state to one ligand. In contrast, the LUMO of **PE1-2**, **PE1-3** and **PE2-3** is confined to the more conjugated ligand. Because of strong overlap between the singlet exciton and the triplet exciton, intersystem crossing is predicted to be more efficient in these systems.

Does the distance between the ligands affect the localization of the triplet state? When electron exchange is small, energy transfer between the two ligands will occur by Forster transfer.[38] As electron exchange increases, energy transfer occurs by the Dexter

mechanism. Finally, the coupling between the ligands is so strong that they behave as a single chromophore. We did DFT calculations on **PE1-BD**, and find the triplet state is symmetrically delocalized throughout the chromophore. In the platinum complexes, the greater distance between the two ligands decreases their coupling. The triplet state can potentially reside on either ligand, having energies E_{Ta} and E_{Tb}. Intersystem crossing can result in the triplet exciton residing on either ligand. Intramolecular triplet energy transfer occurs between ligand **a** and ligand **b** via Dexter coupling, resulting in phosphorescence only from ligand **b**.[39]

Figure 8 gives a Jablonski diagram summarizing our results. In **PEa-b** chromophores, the S_0 and S_1 states are delocalized through the entire molecule. Intersystem crossing results in the T_1 exciton being localized on the higher energy ligand **a** or ligand **b**. The T_1 exciton localized on ligand **a** then undergoes energy transfer to ligand **b**. Phosphorescence occurs from ligand **b**. A similar result from the literature describes photoluminescence from a platinum acetylide polymer containing both phenyl and thiophene monomer units. Most of the emission comes from the lower energy thiophene units, but some emission is also observed from the higher energy phenyl units.[40] The study describes similar excited state dynamics, where intersystem crossing results in the T_1 exciton residing on the phenyl unit with some phosphorescence from the phenyl, followed by energy transfer to the thiophene unit and subsequent phosphorescence from the thiophene unit.

During intersystem crossing, the reaction coordinate for distortion of the molecule moves towards the critical geometry involved in the nonadiabatic transition between the singlet and triplet potential energy surfaces.[29] Because of symmetry, the molecular

orbitals are delocalized through the molecule and the ground and singlet states have a single minimum along the reaction coordinate. In contrast, the lower symmetry triplet exciton has a double minimum.[14] It can reside in either ligand, with energy transfer between the ligands. In **PEn**, the two minima have the same energy. In the asymmetric **PEa-b** chromophores, our experimental and computational results show the triplet exciton resides in the more conjugated, lower energy ligand, giving evidence for a double minimum with different energies. The triplet state energy difference ΔE_{Tab} between **PE2** and **PE3** ligands is 0.12 eV, small enough for thermal equilibration of the triplet exciton to occur between the two ligands, resulting in weak emission from the **PE2** ligand as well as the **PE3** ligand in **PE2-3**. As the difference approaches 0, we would expect to see phosphorescence from both ligands.

CONCLUSIONS

We have synthesized the asymmetric complexes **PE1-2**, **PE1-3** and **PE2-3** and have determined various spectroscopic trends. The singlet state energy E_S decreases with increasing chromophore length, giving evidence that the singlet state is delocalized through the platinum, while the triplet state energy E_T is a function of the longest ligand. The E_T trends suggest that the intersystem crossing mechanism involves movement of the triplet exciton to the lowest energy ligand. We also performed DFT calculations and determined trends in the triplet state geometry and energy. Our calculated E_T energies correlate well with the experimental values. The calculated triplet state geometry shows the geometry changes occur only on the lowest energy ligand. Spin density calculations also show the triplet state is confined to one ligand. Future work will focus on the structure changes occurring on a sub-picosecond time scale following excitation.[41]

ACKNOWLEDGEMENT

The authors thank Jean-Philippe Blaudeau and Gary Kedziora and Kiet Nguyen for very helpful guidance in DFT calculations and Edward Lim for insightful discussions on the triplet state potential energy surface.

SUPPORTING INFORMATION AVAILABLE

Complete results of the TDDFT calculations are available free of charge via the Internet at http://pubs.acs.org.

REFERENCES

(1) Rogers, J. E.; Cooper, T. M.; Fleitz, P. A.; Glass, D. J.; McLean, D. G. *J. Phys. Chem. A* **2002,** *106*, 10108-10115.

(2) Liu, Y.; Jiang, S.; Glusac, K. D.; Powell, D. H.; Anderson, D. F.; Schanze, K. S. *J. Amer. Chem. Soc.* **2002,** *124*, 12412-12413.

(3) Kohler, A.; Wilson, J. S.; Friend, R. H.; Al-Suti, M. K.; Khan, M. S.; Gerhard, A.; Bassler, H. *J. Chem. Phys.* **2002,** 116, 9457-9463.

(4) Bruce, M. I.; Davy, J.; Hall, B. C.; Jansen van Galen, Y.; Skelton, B. W.; White, A. H. **2002,** *16*, 559-568.

(5) Szafert, S.; Gladysz, J. A. *Chem. Rev.* **2003,** *103*, 4175-4205.

(6) Emmert, L. A.; Choi, W.; Marshall, J. A.; Yang, J.; Meyer, L. A.; Brozik, J. A. *J. Phys. Chem. A* **2003,** *107*, 11340-11346.

(7) Yam, V. W.-W. *Acc. Chem. Res.* **2002,** *35*, 555-563.

(8) Cooper, T. M.; Hall, B. C.; Burke, A. R.; Rogers, J. E.; McLean, D. G.; Slagle, J. E.; Fleitz, P. A.. *Chem. Mater.* **2004,** *16*, 3215-3217.

(9) Cooper, T. M. *Encyclopedia of Nanomaterials and Nanotechnology*, Nalwa, H. S., Ed. American Scientific Publishers: **2004**; *10*, pp 447-470.

(10) Cooper, T. M.; McLean, D. G.; Rogers, J. E. *Chem. Phys. Lett.* **2001,** *349*, 31-36.

(11) Rogers, J. E.; Hall, B. C.; Hufnagle, D. C.; Slagle, J. E.; Ault, A. P.; McLean, D. G.; Fleitz, P. A.; Cooper, T. M. *J. Chem. Phys.* **2005,** *122*, 214708-214715.

(12) Cooper, T. M.; Krein, D. M.; Burke, A. R.; McLean, D. G.; Rogers, J. E.; Slagle, J. E. *J. Phys. Chem A* **2006,** *110*, 4369-4375.

(13) Cooper, T. M.; Blaudeau, J.-P.; Hall, B. C.; Rogers, J. E.; McLean, D. G.; Liu, Y.; Toscano, J. P. *Chem. Phys. Lett.* **2004,** *400*, 239-244.

(14) Batista, E. R.; Martin, R. L.. *J. Phys. Chem A* **2005**,*109*, 9856-9859.

(15) Frisch, M. J.; Trucks, G. W.; Schlegel, H. B.; Scuseria, G. E.; Robb, M. A.; Cheeseman, J. R.; Montgomery, J. A.; Vreven, T.; Kudin, K. N.; Burant, J. C.; Millam, J. M.; Iyengar, S. S.; Tomasi, J.; Barone, V.; Mennucci, M.; Cossi, G.; Scalmani, G.; Rega, N.; Petersson, A. S.; Nakatsuji, H.; Hada, M.; Ehara, M.;

Toyota, K.; Fukuda, R.; Hasegawa, J.; Ishida, M.; Nakajima, T.; Honda, Y.; Kitao, O.; Nakai, H.; Klene, M.; Li, X.; Knox, J. E.; Hratchian, H. P.; Cross, J. B.; Adamo, C.; Jaramillo, J.; Gomperts, R.; Stratmann, R. E.; Yazyev, O.; Austin, A. J.; Cammi, R.; Pomelli, C.; Ochterski, J. W.; Ayalo, P. Y.; Morokuma, K.; Voth, G. A.; Salvador, P.; Dannenberg, J. J.; Zakrewski, V. G.; Dapprich, S.; Daniels, A. D.; Strain, M. C.; Farkas, O.; Malick, D. K.; Rabuck, A. D.; Raghavachari, K.; Foresman, J. B.; Ortiz, J. V.; Cui, Q.; Baboul, A. G.; Clifford, S.; Cioslowski, J.; Stefanov, B. B.; Liu, G.; Liashenko, A.; Piskorz, P.; Komaromi, I.; Martin, R. L.; Fox, D. J.; Keith, T.; Al-Laham, M. A.; Peng, C. Y.; Nanayakkara, A.; Challacombe, M.; Gill, P. M. W.; Johnson, B.; Chen, W.; Wong, M. W.; Gonzaez, C.; Pople, J. A. Revision B.05; Gaussian, Inc.: Pittsburgh, 2003.

(16) Norman, P.; Cronstrand, P.; Ericsson, J. *Chem. Phys.* **2002,** *285*, 202-220.

(17) Baev, A.; Rubio-Pons, O.; Gel'Mukanov, F.; Agren, H. *J. Phys. Chem A* **2004,** *108*, 7406-7416.

(18) Koch, W.; Holthausen, M. C. *A Chemist's Guide to Density Functional Theory.* Wiley-VCH: Weinheim, 2001.

(19) Cooper, T. M.; Hall, B. C.; McLean, D. G.; Rogers, J. E.; Burke, A. R.; Turnbull, K.; Weisner, A. J.; Fratini, A.; Liu, Y.; Schanze, K. S.. *J. Phys. Chem A* **2005,** *109*, 999-1007.

(20) Platt, J. R., *J. Chem. Phys.* **1949**, *17*, 470-481.

(21) Serrano-Andres, L.; Merchan, M.; Jablonski, M. *J. Chem. Phys.* **2003,** *119*, 4294-4303.

(22) Amatatsu, Y.; Hasebe, Y. *J. Phys. Chem A* **2003,** *107*, 11169-11173.

(23) Beljonne, D.; Wittman, H. F.; Kohler, A.; S., G.; Younus, M.; Lewis, J.; Raithby, P. R.; Khan, M. S.; Friend, R. H.; Bredas, J. L.. *J. Chem. Phys.* **1996,** *105*, 3868-3877.

(24) Haskins-Glusac, K.; Ghiviriga, I.; Abboud, K. A.; Schanze, K. S. *J. Phys. Chem. B* **2004,** *108*, 4969-4978.

(25) Nguyen, P.; Lesley, G.; Marder, T. B.; Ledoux, I.; Zyss, J. *Chem. Mater.* **1997,** *9*, 406-408.

(26) Nguyen, K. A.; Kennel, J.; Pachter, R. *J. Chem. Phys.* **2002,** *117*, 7128-7136.

(27) Kim, K.-Y.; Liu, S.; Kose, M. E.; Schanze, K. S., *Inorg. Chem.* **2006,** *49*, 2509-2519.

(28) Tao, C.-H.; Zhu, N.; Yam, V. W.-W. *Chem. Eur. J.* **2005,** *11*, 1647-1657.

(29) Turro, N. J. *Modern Molecular Photochemistry*. University Science Books: Sausalito, 1991.

(30) Freed, K. F. *Acc. Chem. Res.* **1978,** *11*, 74-80.

(31) Dauben, W. G.; Salem, L.; Turro, N. J. *Acc. Chem. Res.* **1975,** *8*, 41-54.

(32) Salem, L.; Leforestiew, C.; Segal, G.; Wetmore, R. *J. Amer. Chem. Soc.* **1975,** *97*, 479-487.

(33) Yarkony, D. R. *J. Phys. Chem A* **2001,** *105*, 6277-6293.

(34) Worth, G. A.; Cederbaum, L. S. *Ann. Rev. Phys. Chem.* **2004,** *55*, 127-158.

(35) Amatatsu, Y. *J. Phys. Chem A* **2006,** *110*, 4479-4486.

(36) Zgierski, M. Z.; Lim, E. C.. *Chem. Phys. Lett.* **2004,** *387*, 352-355.

(37) Amatatsu, Y.; Hosokawa, M. *J. Phys. Chem A* **2004,** *108*, 10238-10244.

(38) Gonzalez, C.; Lim, E. C. *Chem. Phys. Lett.* **2000,** *322*, 282-288.

(39) Tian, H.; Yang, S. *J. Photochem. Photobiol. C: Photochem. Rev.* **2002,** *3*, 67-76.

(40) Schanze, K. S.; Silverman, E. E.; Zhao, X. *J. Phys. Chem B* **2005,** *109*, 18451-18459.

(41) Srinivasan, R.; Feenstra, J. S.; Park, S. T.; Xu, S.; Zewail, A. H. *Science* **2005,** *307*, 558-563.

Table 1. Summary of ^{13}C NMR data

Compound	δ_a[1]	Δ_{ab}[2]	δ_b	Δ_{ba}	Dipole moment[4]
PE1-2	108.0	-0.3	112.4	+0.4	1.153
PE1-3	108.0	-0.3	112.9	+0.5	1.627
PE2-3	111.9	-0.1	112.5	+0.1	0.458
PE1[3]	108.3				
PE2	112.0				
PE3	112.4				

[1]In the asymmetric **PEa-b** complexes, ligand **a** is the left ligand; ligand **b** is the right ligand. Chemical shift is in ppm.
[2]change in chemical shift from reference symmetric complex.
[3]Chemical shift values(δ_{aa}) for symmetric complexes obtained from the literature[19]
[4]Dipole moment(debye) calculated as described in methods.

Table 2. Summary of spectroscopic data

Compound	λ_{max}(GS)[1]	ε_{max}[2]	f[3]	λ_{max}(fl)[4]	λ_{max}(ph)[5]	λ_{max}(TT)[6]
PE1-2	349	57,665	1.34	377	524	590
PE1-3	357	69,414	1.97	403	555	650
PE2-3	359	101,815	2.74	401	553	650

[1]Maximum of ground state absorption spectrum in benzene(nm)
[2]Extinction coefficient($M^{-1}cm^{-1}$)
[3]Oscillator strength was obtained by fitting absorption spectrum to three Gaussians.
[4]Maximum of fluorescence spectrum in benzene(nm). Excitation wavelength 355 nm
[5]Peak of 0-0 band of phosphorescence of complex in methyl-THF glass at 77 K
[6]Peak of triplet state absorption spectrum obtained from flash photolysis experiment.

Table 3 Summary of state energies

Compound	E_S[1,3]	E_T	ΔE_{ST}	E_{TT}
PE1-2	3.44	2.38	1.06	2.10
PE1-3	3.21	2.26	0.95	1.91
PE2-3	3.21	2.26	0.95	1.91
PE1[2]	3.58	2.82	0.76	1.97
PE2	3.29	2.38	0.91	2.14
PE3	3.21	2.26	0.95	1.94

[1]eV

[2]State energies for **PE1**, **PE2** and **PE3** were previously published.

[3]E_S was measured from the intersection of the ground state absorption and fluorescence spectra E_T from the blue edge of the phosphorescence spectrum and.

Table 4. Various DFT Calculation Results

Compound	E_{GS}[1]	E_{TS}[2]	E_T[3]	μ[4]	E_S[5]	f[6]	CI result
PE1	-987.2223	-987.1177	2.85	1.49	4.25	0.10	0.48H →L[7]
PE2	-1601.5540	-1601.4691	2.31	3.17	3.37	2.49	0.67H → L
PE3	-2215.8844	-2215.8046	2.17	5.05	2.96	3.88	0.65H → L
PE1-2	-1294.3882	-1294.3032	2.31	4.55	3.48	1.52	0.66H → L
PE1-3	-1601.5534	-1601.4737	2.17	6.86	3.03	2.08	0.67H → L
PE2-3	-1908.7192	-1908.6394	2.17	5.56	3.02	2.40	0.66H → L

[1]Ground state energy(H) calculated from optimized singlet state geometry. **PE1**, **PE2** and **PE3** are assumed to have C_{2h} symmetry. **PE1-2**, **PE1-3**, and **PE2-3** are assumed to have C_s symmetry.
[2]Triplet state energy(H) calculated from optimized triplet state geometry. All chromophores are assumed to have C_1 symmetry.
[3]E_T (eV) is the difference between triplet state energy and ground state energy.
[4]Triplet state dipole moment(D)
[5]Transition energy(eV) calculated from a TDDFT calculation. In **PE1**, the state shown is state 5. For all others, the state shown is state1.
[6]Oscillator strength
[7]**PE1** also had 0.48 H -1 → L+1

Table 5. Bond Length Data for Ground State and Triplet State

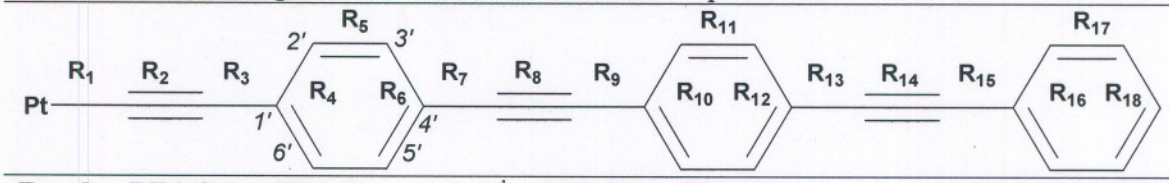

Bond	PE1(S_0)	PE1(T_1)	Δ[1]	PE2(S_0)	PE2(T_1)	Δ	PE3(S_0)	PE3(T_1)	Δ
R_1	2.016	1.975	-0.041	2.014	1.993	-0.021	2.014	2.002	-0.012
R_2	1.242	1.285	0.043	1.243	1.264	0.021	1.243	1.253	0.010
R_3	1.438	1.370	-0.068	1.434	1.392	-0.042	1.434	1.411	-0.023
R_4	1.421	1.480	0.059	1.423	1.464	0.041	1.423	1.444	0.021
R_5	1.405	1.380	-0.025	1.399	1.370	-0.029	1.399	1.380	-0.019
R_6	1.410	1.439	0.029	1.421	1.470	0.049	1.421	1.455	0.034
R_7				1.431	1.377	-0.054	1.430	1.378	-0.052
R_8				1.229	1.255	0.026	1.229	1.262	0.033
R_9				1.433	1.405	-0.028	1.430	1.378	-0.052
R_{10}				1.420	1.435	0.015	1.421	1.456	0.035
R_{11}				1.404	1.399	-0.005	1.398	1.379	-0.019
R_{12}				1.409	1.415	0.006	1.421	1.445	0.024
R_{13}							1.431	1.405	-0.026
R_{14}							1.228	1.239	0.011
R_{15}							1.433	1.422	-0.011
R_{16}							1.420	1.425	0.005
R_{17}							1.404	1.402	-0.002
R_{18}							1.409	1.411	0.002

PE Unit[2]	RMS_1[3]	RMS_2	RMS_3
1	0.044	0.039	0.023
2		0.023	0.035
3			0.010

[1]Bond length change(Å) from ground to triplet state.
[2]Phenyl acetylene unit 1 is closest to the platinum atom
[3]RMS bond length change(Å). Subscript refers to number of phenyl acetylene units in ligand.

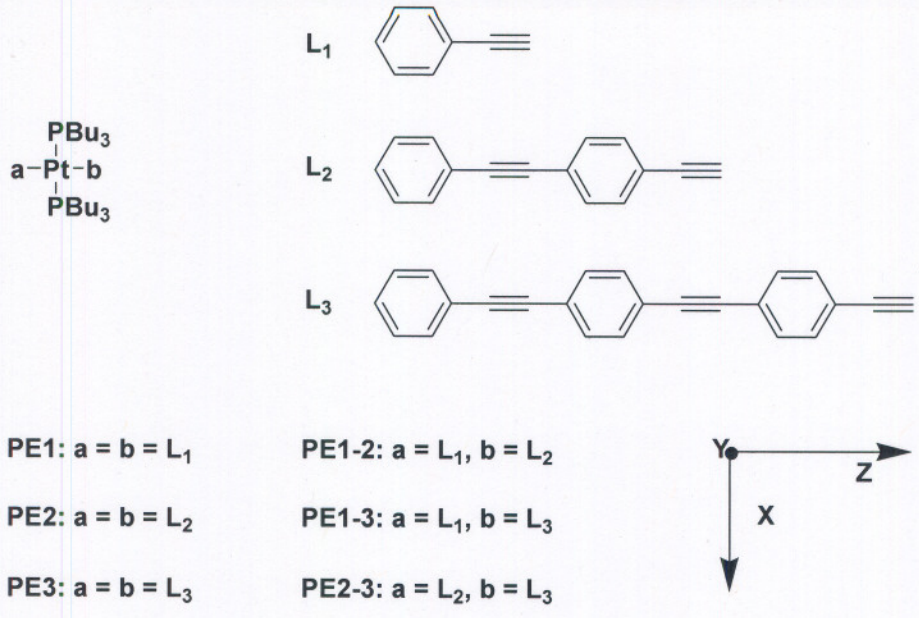

Figure 1. Chemical formulas and nomenclature. Arrows show molecular axes. Nomenclature for the asymmetric compound **a**-Pt(PBu_3)$_2$-**b** , designated as **PEa-b**, labels two ligands of the compound. In discussions below, ligand **a** is designated as the "left ligand" and ligand **b** is the "right ligand". When **a** = Cl, the chromophore is designated as "**half-PEb**".

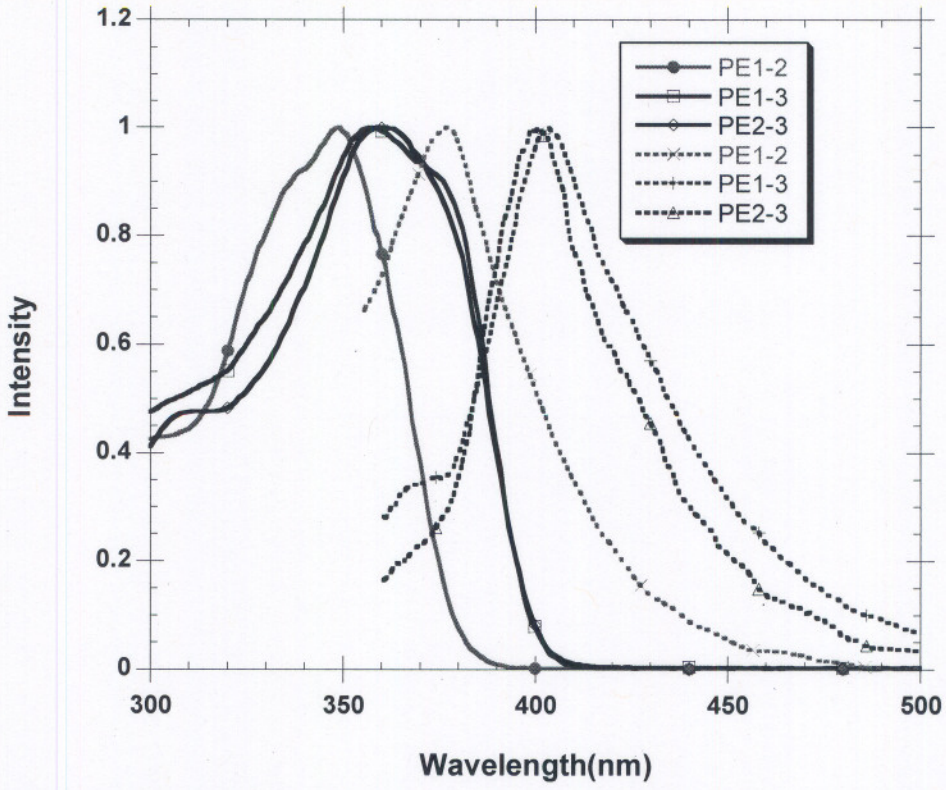

Figure 2. Ground state absorption and emission spectra of the complexes dissolved in benzene. The excitation wavelength was 350 nm.

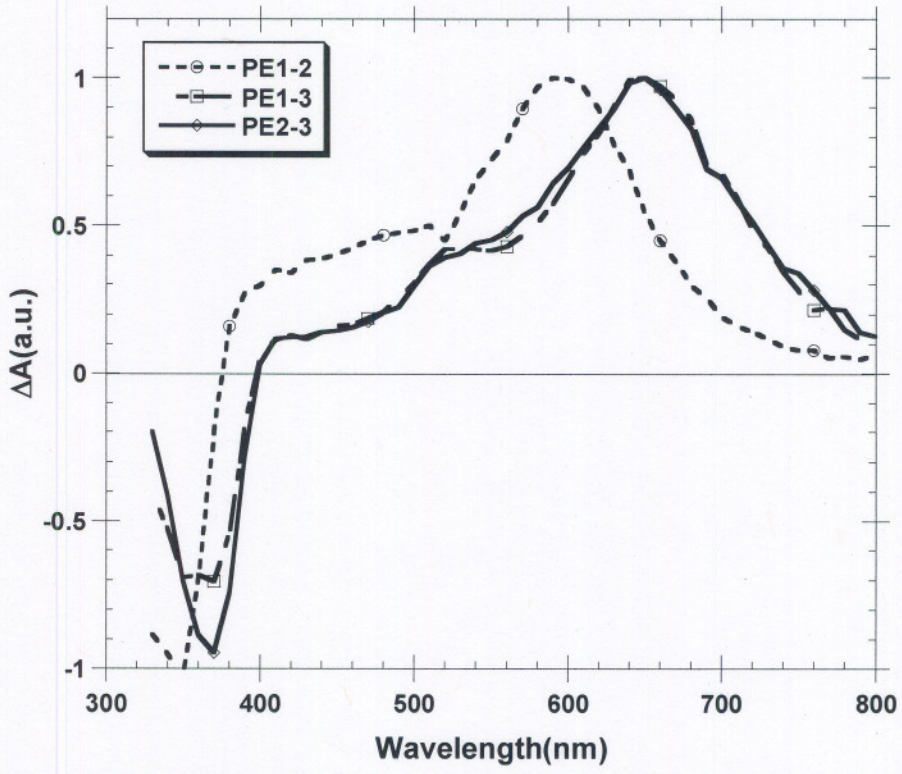

Figure 3 Triplet state absorption spectra obtained from excitation at 355 nm of a degassed benzene solution.

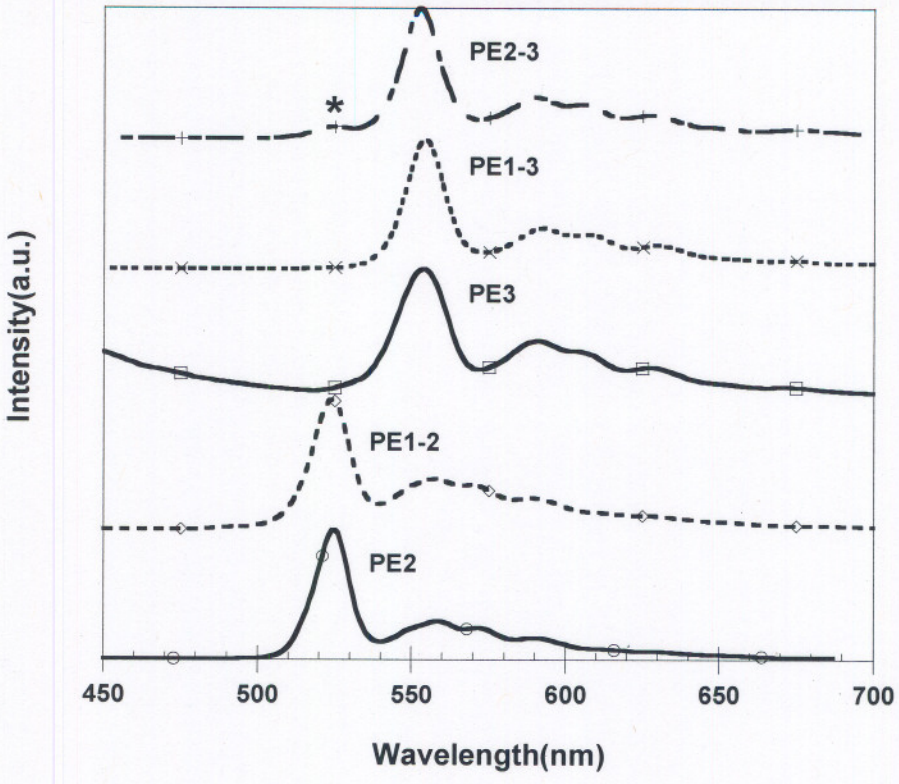

Figure 4. Phosphorescence spectra of chromophores dissolved in methyl-tetrahydrofuran glass at 77 deg K resulting from excitation at 350 nm. Peak marked with an asterisk is weak emission from the **PE2** ligand of **PE2-3**.

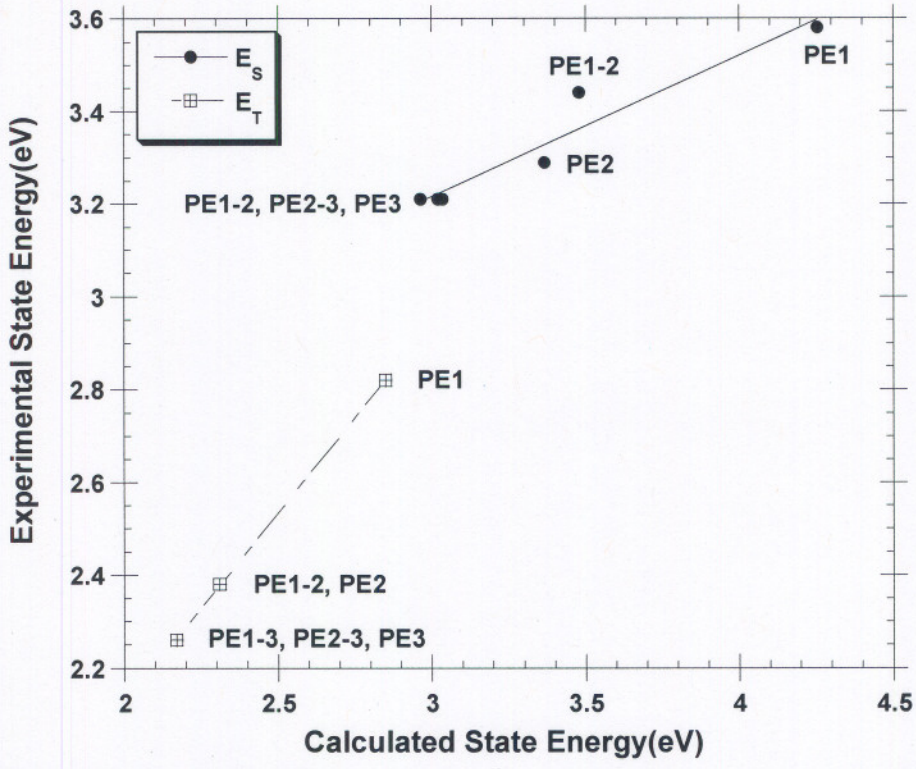

Figure 5 Comparison of calculated and experimental state energies. The triplet state energy E_T was calculated by the ΔSCF DFT method. The singlet state energy was calculated by TDDFT method.

	HOMO	LUMO
PE1		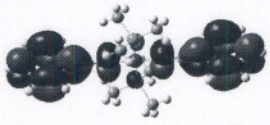
PE2	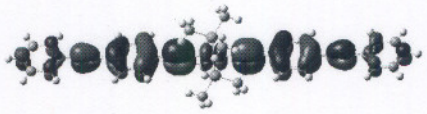	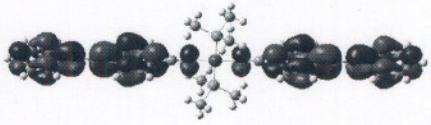
PE3	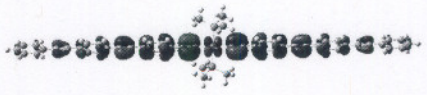	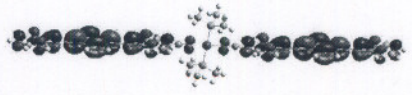
PE1-2	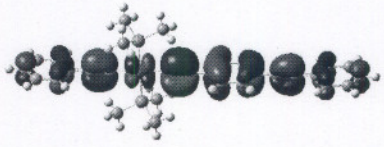	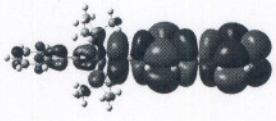
PE1-3		
PE2-3		

Figure 6. Frontier molecular orbitals of the various compounds obtained from DFT calculations of geometry optimized structure.

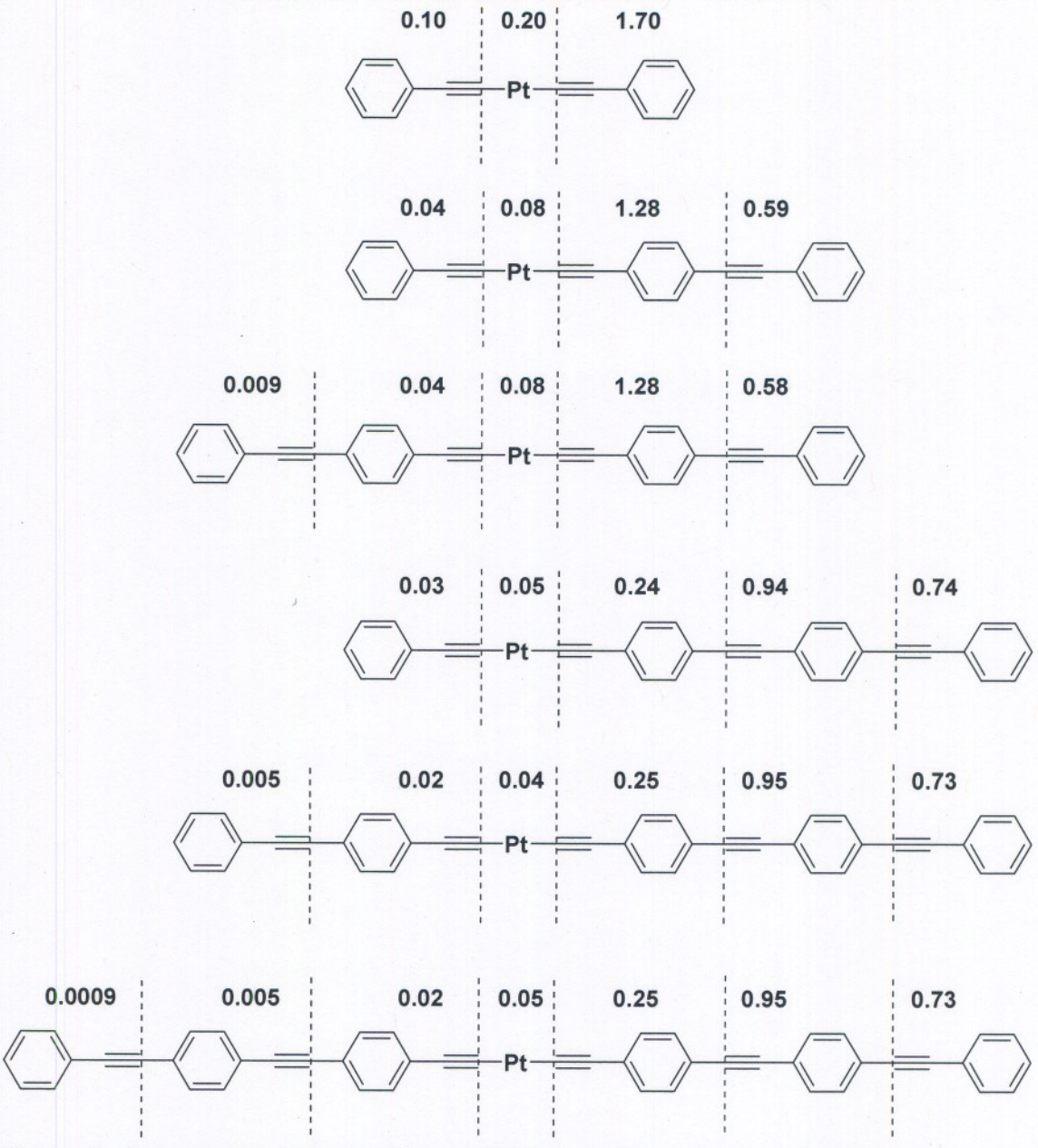

Figure 7. Spin densities obtained from DFT calculations of triplet state optimized geometry. Numbers are the sum of atomic spin density of each phenyl ethynyl or platinum phosphine group.

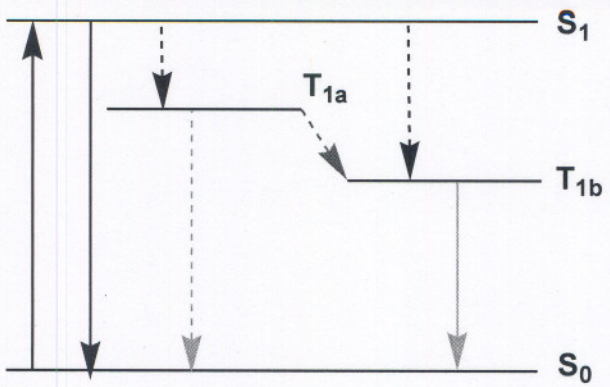

Figure 8. Jablonski diagram that summarizes the spectroscopic behavior. Upon ground state absorption, conversion from the S_0 to the S_1 state occurs(black arrow) . Along with fluorescence(blue arrow), the intersystem crossing process results in the S_1 state splitting into two T_1 states(dotted black arrows). Triplet-triplet energy transfer occurs from the higher energy to lower energy triplet state(dotted red arrow). Phosphorescence predominantly occurs from the lower energy T_{1b} state(green arrow). When the energy difference between the two T_1 states is small, phosphorescence also occurs from the higher energy T_{1a} state(dotted green arrow).

SUPPLEMENTARY MATERIAL FOR

ASYMMETRY IN PLATINUM ACETYLIDE COMPLEXES: CONFINEMENT OF THE TRIPLET EXCITON TO THE LOWEST ENERGY LIGAND

Thomas M. Cooper*[,†], Douglas M. Krein[†,‡], Aaron R. Burke[†,‡], Daniel G. McLean[†,§], Joy E. Rogers[†,#], Jonathan E. Slagle[†,+]

PE1 Excited States

Excitation energies and oscillator strengths:

Excited State 1:	Singlet-BG	4.0542 eV	305.81 nm	f=0.0000	
93 -> 98	0.68672				
Excited State 2:	Singlet-AU	4.0558 eV	305.70 nm	f=0.0001	
94 -> 96	0.69358				
Excited State 3:	Singlet-AG	4.0924 eV	302.96 nm	f=0.0000	
85 -> 98	0.10471				
94 -> 98	0.69063				
Excited State 4:	Singlet-AU	4.1059 eV	301.97 nm	f=0.0000	
90 -> 97	-0.13821				
93 -> 95	0.68262				
Excited State 5:	Singlet-BU	4.2533 eV	291.50 nm	f=0.1011	
93 -> 96	0.48722				
94 -> 95	0.47570				
Excited State 6:	Singlet-BG	4.2960 eV	288.60 nm	f=0.0000	
90 -> 95	-0.18796				
93 -> 97	0.67335				
Excited State 7:	Singlet-BG	4.5064 eV	275.13 nm	f=0.0000	
92 -> 96	-0.69762				
Excited State 8:	Singlet-AU	4.5832 eV	270.52 nm	f=0.0150	
88 -> 97	0.18972				
89 -> 95	0.20971				
92 ->100	-0.26392				
94 -> 99	0.59165				
Excited State 9:	Singlet-BG	4.5834 eV	270.50 nm	f=0.0000	
88 -> 95	0.21155				
89 -> 97	0.18783				
92 -> 99	-0.26609				
94 ->100	0.59038				

PE2 Excited States

Excitation energies and oscillator strengths:

```
 Excited State   1:   Singlet-BU     3.3658 eV  368.37 nm  f=2.4943
     146 ->147         0.66935

 Excited State   2:   Singlet-AU     3.5291 eV  351.32 nm  f=0.0000
     144 ->147         0.68504
     144 ->155         0.12584

 Excited State   3:   Singlet-AG     3.5580 eV  348.46 nm  f=0.0000
     145 ->147        -0.15786
     146 ->148         0.66867

 Excited State   4:   Singlet-BG     3.6413 eV  340.50 nm  f=0.0000
     140 ->147         0.11500
     144 ->148         0.68174
     144 ->156         0.12487

 Excited State   5:   Singlet-AG     3.7357 eV  331.89 nm  f=0.0000
     145 ->147         0.65481

 Excited State   6:   Singlet-BU     3.7578 eV  329.94 nm  f=1.0863
     145 ->148         0.67078
     146 ->147        -0.12673
```

PE3 Excited States

Excitation energies and oscillator strengths:

```
 Excited State   1:   Singlet-B      2.9624 eV  418.53 nm  f=3.8800
     197 ->200         0.18022
     198 ->199         0.65235


 Excited State   2:   Singlet-A      3.1069 eV  399.06 nm  f=0.0000
     198 ->200         0.67562

 Excited State   3:   Singlet-A      3.2703 eV  379.12 nm  f=0.0000
     197 ->199         0.67621
     198 ->200        -0.10245

 Excited State   4:   Singlet-B      3.2868 eV  377.21 nm  f=1.0913
     197 ->200         0.65713
     198 ->199        -0.21654

 Excited State   5:   Singlet-A      3.3147 eV  374.05 nm  f=0.0000
     196 ->199         0.67838
     196 ->201        -0.16720

 Excited State   6:   Singlet-B      3.3834 eV  366.45 nm  f=0.0000
     196 ->200         0.68182
     196 ->202        -0.14967
```

PE1-2 excited states

Excitation energies and oscillator strengths:

```
 Excited State   1:   Singlet-A'     3.4796 eV  356.32 nm  f=1.5170
     120 ->121         0.66346

 Excited State   2:   Singlet-A"     3.5320 eV  351.03 nm  f=0.0000
     115 ->121         0.10300
     119 ->121         0.68343
     119 ->127         0.11557

 Excited State   3:   Singlet-A'     3.8512 eV  321.94 nm  f=0.4129
     118 ->121         0.68409

 Excited State   4:   Singlet-A"     4.0244 eV  308.08 nm  f=0.0000
     118 ->123        -0.14849
     120 ->123         0.67932

 Excited State   5:   Singlet-A"     4.0641 eV  305.07 nm  f=0.0000
     119 ->125         0.68742

 Excited State   6:   Singlet-A'     4.0648 eV  305.02 nm  f=0.0000
     116 ->125         0.10730
     118 ->125        -0.17809
     120 ->125         0.66214
```

PE1-3 Excited States

Excitation energies and oscillator strengths:

```
 Excited State   1:   Singlet-A'     3.0334 eV  408.74 nm  f=2.0815
     146 ->147         0.66939

 Excited State   2:   Singlet-A"     3.2758 eV  378.49 nm  f=0.0000
     144 ->147         0.68129
     144 ->148        -0.15549

 Excited State   3:   Singlet-A'     3.4266 eV  361.82 nm  f=0.4462
     145 ->147         0.68909

 Excited State   4:   Singlet-A'     3.8109 eV  325.34 nm  f=0.4939
     143 ->147         0.58479
     146 ->148        -0.36602

 Excited State   5:   Singlet-A"     4.0262 eV  307.95 nm  f=0.0000
     145 ->150        -0.21680
     146 ->150         0.65808

 Excited State   6:   Singlet-A"     4.0789 eV  303.96 nm  f=0.0000
     129 ->153        -0.10305
     144 ->153        -0.68492
```

PE2-3 Excited States

Excitation energies and oscillator strengths:

```
 Excited State   1:   Singlet-A'     3.0183 eV  410.77 nm  f=2.4036
     171 ->173         0.10180
     172 ->173         0.66108


 Excited State   2:   Singlet-A'     3.2973 eV  376.02 nm  f=0.7315
     171 ->173         0.66780
     172 ->173        -0.15458

 Excited State   3:   Singlet-A"     3.3276 eV  372.59 nm  f=0.0000
     170 ->173         0.67662
     170 ->175        -0.15434

 Excited State   4:   Singlet-A'     3.4782 eV  356.46 nm  f=0.5090
     172 ->174         0.66333

 Excited State   5:   Singlet-A"     3.6018 eV  344.23 nm  f=0.0000
     166 ->174        -0.10237
     170 ->174         0.67904
     170 ->183         0.11717

 Excited State   6:   Singlet-A'     3.7184 eV  333.44 nm  f=0.6691
     171 ->174         0.66557
```